mater.scichina.com link.springer.com

Published online 31 July 2020 | https://doi.org/10.1007/s40843-020-1466-0
Sci China Mater 2021, 64(1): 46–51

The rise of plastic deformation in boron nitride ceramics

Yingju Wu[1†], Yang Zhang[1,2†], Shuangshuang Zhang[1†], Xiaoyu Wang[1], Zitai Liang[1], Wentao Hu[1], Zhisheng Zhao[1*], Julong He[1], Dongli Yu[1], Bo Xu[1], Zhongyuan Liu[1] and Yongjun Tian[1*]

Ceramics are bonded by ionic or covalent bonds, with very limited slip systems for dislocation nucleation and movement [1]. The poor deformability and natural brittleness are the major drawbacks of ceramics, especially when compared with metals. Under stress, ceramics tend to fracture before noticeable plastic deformation takes place. Cracks occur and propagate rapidly in ceramics subjected to stress much lower than the theoretical strength [2]. As a result, ceramics can only endure very small strains (<1%), absorb limited mechanical energy, and display poor toughness [3]. Moreover, microstructure imperfections in ceramics may decrease the toughness even further. Due to the lack of significant plastic deformation capacity for ceramic materials, the catastrophic failures without warning are easy to happen under stress which critically increases the unreliability of ceramics in the applications as structural materials.

Compared with traditional ceramics with a rigid structure, ceramics with a layered atomic structure and relatively weak interactions between atomic layers might possess a promoted capability in deformation, with contributions from a range of deformation modes, such as basal slip, kink and shear band deformations, and grain delamination [4–6]. Typical ceramics of this type include graphite and MAX phases [7,8]. Polycrystalline graphite shows a compressive strength up to 100 MPa and fracture strain less than 2.2%, with a residual plastic strain less than 0.2% [9]. MAX (the ternary carbides and nitrides with the general formula $M_{n+1}AX_n$ (MAX)—where n = 1, 2, or 3; M is an early transition metal; A is an A-group element (a subset of group 13–16 elements); and X is C and/or N) phase ceramics with fine grains usually show a brittle nature and tend to fracture under small compressive strains, e.g., Ti_2AlC fractures under strain of 1.2%, with a maximum residual strain of 0.55% [10]. Ti_3SiC_2 with oriented millimeter-sized grains displays improved compression ductility [11]. However, the yield strength (ca. 200 MPa) is significantly reduced, only one-fifth of that of the fine-grained Ti_3SiC_2 ceramics [11,12]. It is a great challenge to simultaneously improve the deformability and strength of ceramics with a layered atomic structure.

Hexagonal boron nitride (hBN) possesses a layered atomic structure similar to graphite [13]. It has an excellent combination of chemical and physical properties, such as high thermal conductivity, thermal shock resistance, ablation resistance, and thermal and chemical stability, and thus it is widely used in many fields such as metallurgy, automotive industry and aerospace [14,15]. However, hBN ceramics show inferior mechanical properties, which arouse numerous research efforts recently [16–20]. The compressive strength of the densified hBN ceramics prepared with spark plasma sintering (SPS) is limited to about 100 MPa [20]. Meanwhile, the deformation behaviors of the hBN ceramics are essentially left out. In this study, the hBN ceramic samples were fabricated with SPS with two precursors, onion-like BN (oBN) nanoparticles and hBN nanoplates. The ceramic from oBN nanoparticles (BN-I) is constructed with randomly oriented nanolaminae interlocked into a three-dimensional (3D) structure, exhibiting a compressive strength as high as 343 MPa and fracture strain up to 4.2%. In comparison, the ceramic from hBN nanoplates (BN-II) is made of micron-sized laminae with a preferred orientation, and shows inferior mechanical properties compared with BN-I. Both samples display an obvious

[1] Center for High Pressure Science (CHiPS), State Key Laboratory of Metastable Materials Science and Technology, Yanshan University, Qinhuangdao 066004, China
[2] Key Laboratory for Microstructural Material Physics of Hebei Province, Yanshan University, Qinhuangdao 066004, China
† These authors contributed equally to this work.
* Corresponding authors (emails: zzhao@ysu.edu.cn (Zhao Z); fhcl@ysu.edu.cn (Tian Y))

residual deformation (plastic deformation) up to 1.1% after decompression.

To produce dense ceramics, home-made oBN nanoparticles [21] and hBN nanoplates (Alfa Aesar) were sintered in an SPS apparatus (SPS-3.20 MK-IV, Syntex Inc., Japan) at 50 MPa for 10 min, with the temperature of 1700°C and 1800°C, respectively. The densities of BN-I and BN-II ceramics are 2.07 and 2.08 g cm^{-3}, respectively, which are slightly lower than the theoretical density of hBN (2.27 g cm^{-3}). The phase composition of the BN-I and BN-II ceramics along with the precursors was determined by X-ray diffraction (XRD, Smartlab Rigaku with Cu-Kα radiation), as shown in Fig. 1. A remarkable difference is observed in the XRD patterns for BN-I and oBN (Fig. 1a), indicating substantial structural transformation during sintering. oBN precursors show broad peaks at 24°–26° and 40°–45°, related to the turbostratic layered structure in oBN. This is consistent with the transmission electron microscopy (TEM) observation of oBN nanoparticles where multilayered concentric spheres of intrinsically puckered BN layers and numerous stacking faults are revealed [21–23]. XRD patterns of the BN-I ceramic show similar character with that of hBN. For example, the broad peak at 24°–26° for oBN becomes narrowed and shifts to higher angle in BN-I, with an interlayer spacing of 0.334 nm corresponding to the (002) *d*-spacing of hBN [13]. In comparison, there is no obvious difference in XRD patterns of hBN nanoplate precursors and BN-II ceramic (Fig. 1b), and both of them are dominated by the hBN phase.

XRD patterns were collected from the ceramic surfaces perpendicular (Fig. 1, red curves) and parallel (blue curves) to the uniaxial compressing direction of SPS. The index of orientation preference (IOP) calculated from (002) and (100) diffractions of hBN reveals an important difference between the BN-I and BN-II ceramics [24]. IOP values of BN-I and BN-II are −1.6 and −6.2, respectively. Therefore, hBN grains in BN-II ceramic are preferentially oriented with the basal planes perpendicular to the compressing direction of SPS, while the grains in BN-I ceramic are more randomly oriented. Such a difference in texture can be attributed to the form of precursors. During SPS sintering, the anisotropic hBN nanoplates (see Fig. 2c for the morphology) tend to align with the lateral flow, with the basal plane perpendicular to the compressing direction [25]. oBN nanoparticles (Fig. 2a), however, go through a transition to layered structure under suitable temperature and pressure. Due to the isotropic spherical shape of the nanoprecursor, the generated grains would be randomly oriented and mutually restrained.

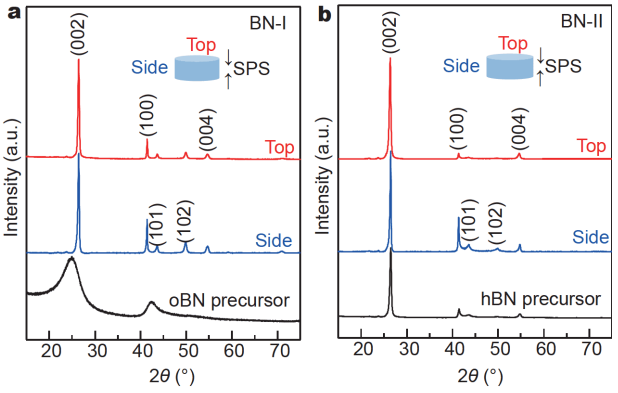

Figure 1 XRD patterns of the BN-I and BN-II ceramics and the corresponding precursors. (a) BN-I and oBN. (b) BN-II and hBN nanoplates. XRD patterns were acquired from top and side surfaces of the ceramics (see the inset for the positioning).

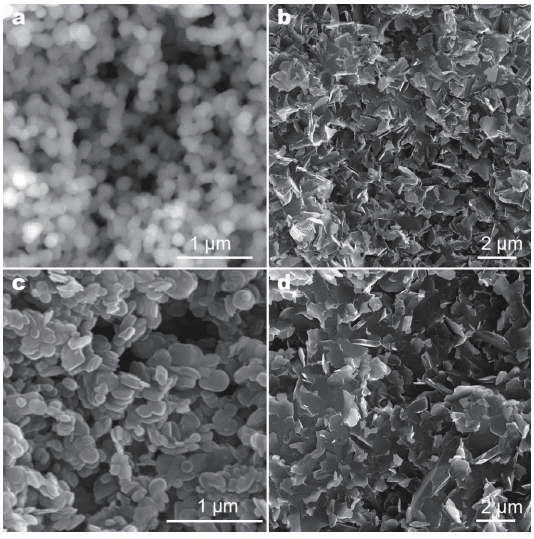

Figure 2 SEM images of the precursors and SPS ceramics. (a) Spherical oBN nanoparticles. (b) Freshly fractured surface of BN-I ceramic. (c) hBN nanoplate precursor. (d) Freshly fractured surface of BN-II ceramic. The ceramic surface was covered with a thin layer of Pt film by ion-sputtering before the SEM observation.

The morphology and microstructure of the precursors and ceramics were characterized with scanning electron microscopy (SEM, SCIOS FEI, USA). The spherical oBN nanoparticles show an average particle size of ca. 200 nm (Fig. 2a), and the hBN nanoplates show a lateral size of ca. 180 nm and a thickness of tens of nanometers (Fig. 2c). After sintering, both ceramics show grains in a laminar shape, with difference in preferred orientation though. In BN-I, nanolaminae with an average width of ca. 700 nm are randomly distributed (Fig. 2b), while in BN-II, thin

nanosheets, ca. 600 nm in width, are packed into micron-sized regions that are preferentially oriented (Fig. 2d). The observed microstructure further verifies the different texture revealed by the XRD results.

Uniaxial compression tests were performed on cylindrical specimens of the SPS ceramics (Fig. 3). Two specimens were prepared for each ceramic, perpendicular (⊥) and parallel (//) to the compressing direction of SPS. A thin copper foil was placed between the cylinder tops and loading plates to alleviate the edge effects. The compression process was monitored with a digital image correlation system (Mercury RT, Sobriety SRO, Czech). The compression strain rate was set to 1×10^{-4} s^{-1}. The compressive stress-strain curves of BN-I and BN-II indicate a nonlinear compression characteristic (Fig. 3a), distinct from the traditional technical ceramics (e.g., SiC, MgO, Al_2O_3, Si_3N_4, etc.), which comes from the unique deformation modes in the layered materials including the formation of ripplocation, buckling, and kink bands [5,6,26,27]. The compressive strength of BN-$I_{//}$ reaches 343 MPa, three times that of BN-$II_{//}$ (112 MPa). The corresponding fracture strain of BN-$I_{//}$ is 4.2%, nearly double that of BN-$II_{//}$ (2.2%). In the direction perpendicular to the sintering pressure, BN-I and BN-II show slightly degraded strength and deformability. The compressive strengths for BN-$I_{\perp}$ and BN-$II_{\perp}$ are 295 and 82 MPa, with fracture strains of 3.8% and 1.9%, respectively.

The cyclic compression/decompression curves of BN-$I_{//}$ and BN-$II_{//}$ specimens are shown in Fig. 3b, c, respectively. Note the final failure cycle is not shown. Two common characteristics are revealed from the stress-strain curves for both ceramics: (i) the hysteresis loop appears from the beginning of load-unload cycles; (ii) small plastic deformation occurs even after the first cycle, as indicated by the residual strain. Similar reversible hysteresis loops have been observed in MAX phase ceramics, which can be explained by the response of the anisotropic microstructure generating strongly varied microstrains in every grain [28]. The plastic deformation can be attributed to the accumulated irreversible damages in the forms of kink bands, delamination and cracks which occur during compression [4]. BN-$I_{//}$ can be cyclically compressed to 330 MPa with a corresponding

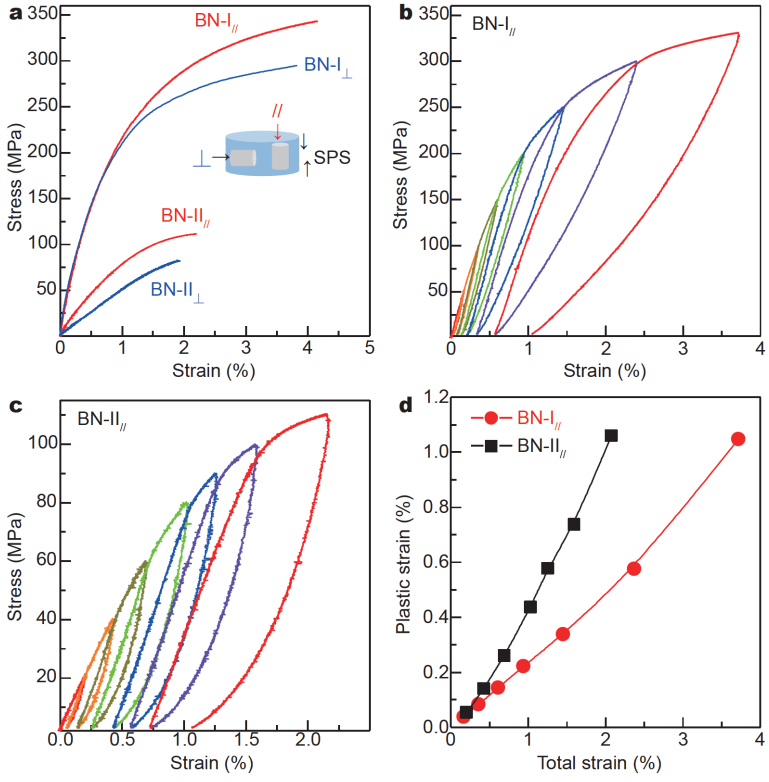

Figure 3 Uniaxial compression characterization of the BN ceramics. (a) Single compressive stress-strain curves of BN-I and BN-II. Cylindrical specimens (Φ3 mm×4.5 mm) were cut from the SPS plate perpendicular (⊥) and parallel (//) to the compressing direction of SPS. (b) Cyclic stress-strain curves of BN-$I_{//}$ specimen. (c) Cyclic stress-strain curves of BN-$II_{//}$ specimen. (d) Plastic strain as a function of total strain, indicating a smaller plastic strain component in the total strain for BN-I than that for BN-II.

strain of 3.7%, while BN-II$_{//}$ can be compressed to 110 MPa with a strain of 2.2%. For each cycle, the total strain is compared with the corresponding residual plastic strain after unloading (Fig. 3d). The plastic strain for both ceramics increases up to 1.1% with elevated total strain. With the same total strain, BN-I clearly shows a smaller plastic component compared with BN-II, implying much less irreversible damage accumulated in BN-I. In addition, a strength degradation is revealed in BN-II when the applied stress is higher than 60 MPa, which can also be attributed to the accumulated damage during the load-unload cycles. In comparison, BN-I does not show obvious strength degradation even at the highest stress of 300 MPa, highlighting excellent damage tolerance.

To understand the different compressive behaviors of BN-I and BN-II, the morphology of the fractured surface after compression test was analyzed with SEM (Fig. 4). For BN-I, the fractured surface shows randomly arranged BN nanoflakes with a 3D interlocked structure. In this configuration, the slips in and between individual nanoflakes can be confined by the surrounding nanoflakes with different orientations, resulting in a high compressive strength. Due to such a confinement effect, thin nanoflakes may also deform flexibly under external stress, and contribute to a substantial deformability of the BN-I ceramic. The deformation may occur with the formation of kink bands (see the bent BN nanoflakes marked with red arrows in Fig. 4b), similar to MAX phase ceramics under compression [6]. For BN-II, the cleavage planes with size of several microns are recognized (Fig. 4c). Closer examination indicates these cleavage micron-sized laminae are actually composed of numerous highly-aligned nanosheets (see the green loops in Fig. 4d). The failure mode of BN-II is similar to that of the ordinary hBN ceramics [18,20], with an enhanced strength and deformability though.

To achieve room-temperature high strength and large deformability simultaneously in ceramics is considered as a tough challenge. However, the BN-I and BN-II ceramics with a layered atomic structure produced in this study specify a feasible pathway to plastic ceramics. The uniaxial compression tests reveal the enhanced compressive strength, substantial plastic deformation, and a nonlinear compression character different from the traditional ceramics. BN-I from the oBN nanoparticles shows a high compressive strength of 343 MPa and a large fracture strain of 4.2%. BN-II from the hBN nanoplates shows a compressive strength of 112 MPa, which is comparable to the best of ordinary hBN ceramics, and a strain of 2.2%. A plastic strain as high as 1.1% is achieved in both BN-I and BN-II. The microstructure characterizations reveal that 3D interlocked architecture with randomly oriented nanolaminae plays an essential role for enhanced strength and deformability. This study sheds light on future developments of plastic ceramics, with current strategy applicable to other ceramics with similar atomically layered structure.

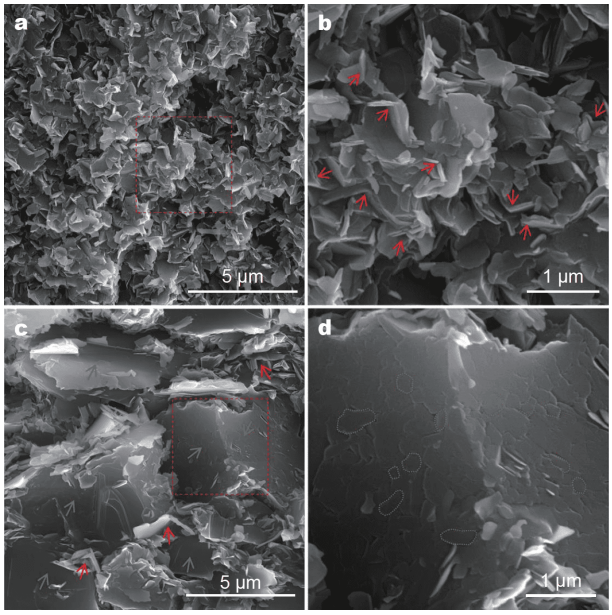

Figure 4 SEM images of the fractured surfaces of BN-I and BN-II after compression test. A thin layer of Pt film was ion-sputtered on the fractured surfaces of BN ceramics before the SEM observation. (a) BN-I. (b) SEM micrograph from the red-framed region in (a). Randomly oriented nanolaminae in BN-I are interlocked into 3D architecture. (c) BN-II. (d) SEM micrograph from the red-framed region in (c). Micron-sized cleaved planes are revealed in BN-II, which are composed of highly-aligned nanosheets, as emphasized with the green loops. Red arrows mark the bent nanoflakes with the formation of kink bands; green arrows sign the cleaved micron-sized laminae.

Received 22 June 2020; accepted 20 July 2020; published online 31 July 2020

1 Carter CB, Norton MG. Ceramic Materials: Science and Engineering. New York: Springer, 2007
2 Griffith AA. The phenomena of rupture and flow in solids. Philos T R Soc A, 1921, 221: 163–198
3 Green DJ. An Introduction to the Mechanical Properties of Ceramics. Cambridge: Cambridge University Press, 1998
4 Jones NG, Humphrey C, Connor LD, *et al.* On the relevance of kinking to reversible hysteresis in MAX phases. Acta Mater, 2014, 69: 149–161
5 Barsoum MW, Murugaiah A, Kalidindi SR, *et al.* Kink bands, nonlinear elasticity and nanoindentations in graphite. Carbon, 2004, 42: 1435–1445
6 Barsoum MW, Farber L, El-Raghy T. Dislocations, kink bands, and

room-temperature plasticity of Ti_3SiC_2. Metall Mat Trans A, 1999, 30: 1727–1738
7 Barsoum MW, Radovic M. Elastic and mechanical properties of the MAX phases. Annu Rev Mater Res, 2011, 41: 195–227
8 Telling RH, Heggie MI. Stacking fault and dislocation glide on the basal plane of graphite. Philos Mag Lett, 2003, 83: 411–421
9 Seldin EJ. Stress-strain properties of polycrystalline graphites in tension and compression at room temperature. Carbon, 1966, 4: 177–191
10 Poon B, Ponson L, Zhao J, *et al.* Damage accumulation and hysteretic behavior of MAX phase materials. J Mech Phys Solids, 2011, 59: 2238–2257
11 Barsoum MW, El-Raghy T. Room-temperature ductile carbides. Metall Mat Trans A, 1999, 30: 363–369
12 Barsoum MW, Zhen T, Kalidindi SR, *et al.* Fully reversible, dislocation-based compressive deformation of Ti_3SiC_2 to 1 GPa. Nat Mater, 2003, 2: 107–111
13 Pauling L. The structure and properties of graphite and boron nitride. Proc Natl Acad Sci USA, 1966, 56: 1646–1652
14 Sinclair W, Simmons H. Microstructure and thermal shock behaviour of BN composites. J Mater Sci Lett, 1987, 6: 627–629
15 Lipp A, Schwetz KA, Hunold K. Hexagonal boron nitride: Fabrication, properties and applications. J Eur Ceramic Soc, 1989, 5: 3–9
16 Wang TB, Jin CC, Yang J, *et al.* Physical and mechanical properties of hexagonal boron nitride ceramic fabricated by pressureless sintering without additive. Adv Appl Ceramics, 2015, 114: 273–276
17 Ay N, Tore I. Pressureless sintering of hexagonal boron nitride powders. Mater Sci Forum, 2007, 554: 207–212
18 Yang H, Fang H, Yu H, *et al.* Low temperature self-densification of high strength bulk hexagonal boron nitride. Nat Commun, 2019, 10: 854–862
19 Chen L, Wang Y, Shen H, *et al.* Effect of SiC content on mechanical properties and thermal shock resistance of BN–ZrO_2–SiC composites. Mater Sci Eng-A, 2014, 590: 346–351
20 Duan X, Jia D, Wang Z, *et al.* Influence of hot-press sintering parameters on microstructures and mechanical properties of h-BN ceramics. J Alloys Compd, 2016, 684: 474–480
21 Tang C, Bando Y, Huang Y, *et al.* Synthetic routes and formation mechanisms of spherical boron nitride nanoparticles. Adv Funct Mater, 2008, 18: 3653–3661
22 Tian Y, Xu B, Yu D, *et al.* Ultrahard nanotwinned cubic boron nitride. Nature, 2013, 493: 385–388
23 Luo K, Zhang Y, Yu D, *et al.* Small onion-like BN leads to ultrafine-twinned cubic BN. Sci China Mater, 2019, 62: 1169–1176
24 Duan X, Jia D, Wu Z, *et al.* Effect of sintering pressure on the texture of hot-press sintered hexagonal boron nitride composite ceramics. Scripta Mater, 2013, 68: 104–107
25 Xue JX, Liu JX, Xie BH, *et al.* Pressure-induced preferential grain growth, texture development and anisotropic properties of hot pressed hexagonal boron nitride ceramics. Scripta Mater, 2011, 65: 966–969
26 Gruber J, Lang AC, Griggs J, *et al.* Evidence for bulk ripplocations in layered solids. Sci Rep, 2016, 6: 33451
27 Barsoum MW, Tucker GJ. Deformation of layered solids: Ripplocations not basal dislocations. Scripta Mater, 2017, 139: 166–172
28 Guitton A, Van Petegem S, Tromas C, *et al.* Effect of microstructure anisotropy on the deformation of MAX polycrystals studied by *in-situ* compression combined with neutron diffraction. Appl Phys Lett, 2014, 104: 241910

Acknowledgements This work was supported by the National Natural Science Foundation of China (NSFC, 91963203, 51672238, 51772260, 51722209 and 51525205). Zhao Z acknowledges the 100 Talents Plan of Hebei Province (E2016100013), the NSF for the Distinguished Young Scholars of Hebei Province (E2018203349).

Author contributions Tian Y and Zhao Z conceived the project. Wu Y, Zhang Y, Zhang S, Zhao Z, and Tian Y designed the experiments. Wu Y prepared the oBN nanoparticles. Wu Y, Zhang Y and Zhang S conducted the SPS experiments. Wang X, Liang Z, and Hu W performed the SEM characterization. Wu Y, Zhang Y and Zhang S conducted the XRD measurements and uniaxial compression tests. Wu Y, Zhang Y, Zhao Z, Tian Y, Yu D, He J, Xu B and Liu Z analyzed the data. Wu Y, Zhang Y, Zhao Z, Xu B and Tian Y co-wrote the paper. All authors discussed the results and commented on the manuscript.

Conflict of interest The authors declare no conflict of interest.

Yingju Wu is currently a PhD candidate in the Center for High Pressure Science (CHiPS), State Key Laboratory of Metastable Materials Science and Technology, Yanshan University. He obtained his bachelor degree in the School of Materials Science and Engineering, Shandong University of Technology in 2014. His current research focuses on the structure and property regulation of advanced structural ceramics.

Yang Zhang received his PhD degree from Yanshan University in 2017. Then, he worked as a postdoctoral fellow at the School of Science, Yanshan University. His current research interests focus on the advanced structural ceramics, and the design and synthesis of novel metastable materials.

Shuangshuang Zhang is currently a PhD candidate in CHiPS, State Key Laboratory of Matestable Materials Science and Technology, Yanshan University. She obtained her bachelor degree in the School of Materials Science and Engineering, Anhui University of Science and Technology in 2015. Her current research focuses on the design and synthesis of new metastable carbon materials.

Zhisheng Zhao graduated from Jiamusi University with a bachelor's degree in 2007, and received his PhD degree in materials physics and chemistry from Yanshan University in 2012. Currently, he works as a professor in CHiPS, State Key Laboratory of Metastable Materials Science and Technology, Yanshan University. His research focuses on the theoretical design, high-pressure synthesis, and performance regulation of new metastable materials.

Yongjun Tian is a professor at CHiPS, State Key Laboratory of Metastable Materials Science and Technology, Yanshan University. He received his PhD degree from the Institute of Physics, Chinese Academy of Sciences in 1994, and worked as a postdoctoral fellow at the Universitat Jena supported by Humboldt Research Fellowships from 1996 to 1998. His research interests include the design and synthesis of superhard materials and novel metastable materials.

塑性氮化硼陶瓷的兴起

武英举[1†], 张洋[1,2†], 张爽爽[1†], 王小雨[1], 梁子太[1], 胡文涛[1], 赵智胜[1*], 何巨龙[1], 于栋利[1], 徐波[1], 柳忠元[1], 田永君[1*]

摘要 传统陶瓷材料的刚性结构变形能力非常有限, 通常在很小的应变下就发生断裂. 具有层状原子结构的陶瓷, 原子层间存在较弱的相互作用, 因而具有大的变形潜力. 我们以氮化硼(BN)为例, 研究了该类陶瓷的室温压缩行为. 分别以洋葱结构BN纳米颗粒和石墨状六方BN纳米片为原料, 采用放电等离子烧结(SPS)技术分别制备了BN-I和BN-II陶瓷材料. 在BN-I中, 随机取向的BN纳米薄片构成三维互锁的结构, 而在BN-II中, BN纳米薄片表现出垂直于SPS压缩方向的择优取向. BN-I的压缩强度为343 MPa, 断裂应变为4.2%. 相比之下, BN-II的强度和应变分别为112 MPa和2.2%. 不同的微观组织结构导致了BN-I和BN-II压缩性能的差异. 此外, 这两种陶瓷材料均表现出1.1%的塑性变形. 该研究表明, 对于具有层状原子结构的陶瓷, 其纳米片作为结构基元构筑成无(或低)择优取向的三维互锁结构, 有望同时提高其强度和变形能力.

